JOURNAL OF AIRCRAFT
Vol. 43, No. 6, November–December 2006

Simulation of the Electroimpulse De-Icing Process of Aircraft Wings

George N. Labeas,* Ioannis D. Diamantakos,† and Milan M. Sunaric†
University of Patras, 265 00 Rion, Greece

DOI: 10.2514/1.21321

The electroimpulse de-icing system of an aircraft wing leading edge is investigated through the development of a methodology for the numerical simulation of the electroimpulse de-icing process. The principle of electroimpulse de-icing is that the ice is removed due to the leading edge local mechanical vibration, which is induced by an electromagnetic pulse. The numerical simulation methodology is based on a nonlinear transient three-dimensional stress analysis of the ice-covered wing, combined to a de-icing criterion that takes into consideration the tensile and shear stresses at the ice-skin interface. The developed methodology is verified on de-icing experimental tests of an aluminum plate. Afterwards, the methodology is applied to the prediction of de-icing of an aircraft wing leading edge. The dominant process parameters are determined to be the coil number and position, the ice thickness and coverage, the radius of wing curvature, and the electroimpulsive load amplitude. A parametric study is performed to determine the influence of the process parameters on the system effectiveness, defined as the percentage of the de-iced surface over the total leading edge surface. From the results of the parametric study, the possibilities of reducing the weight and energy consumption of the electroimpulse de-icing system can arise.

Nomenclature

a, b	=	coupling parameters for the de-icing criterion
E	=	Young's modulus
F	=	time-dependent coil-induced mechanical force
$F_{\max}$	=	amplitude of the coil-induced mechanical force
f	=	generic function
I_{coil}	=	coil electric current
$ROTX$	=	rotational degree of freedom for x axis
$ROTZ$	=	rotational degree of freedom for z axis
r	=	coil radius
T	=	coil activity period
t	=	coil circuit discharging time
U	=	coil circuit voltage
UY	=	translational degree of freedom for y axis
μ_0	=	magnetic permeability
ν	=	Poisson's ratio
ρ	=	density
σ	=	normal stress
$\sigma_{\max}$	=	maximum normal stress
σU	=	ultimate normal stress
τ_{xz}, τ_{yz}	=	out-of-plane shear stresses
$\tau_{\max}$	=	maximum shear stress
τ_U	=	ultimate shear stress

I. Introduction

A major problem since the earliest days of aeronautics has been the ice accumulation (accretion) on the aircraft aerodynamic surfaces. The in-flight ice accretion occurs on the frontward facing surfaces and usually covers only 2% of the wing chord with an ice layer of a few centimeters thickness. But even this small percentage of ice thickness at critical aircraft locations is enough to cause flow separation and destroy lift [1], reduce the maximum lifting capability and increase drag, affect the control surface effectiveness, and in some cases decrease engine performance and stability [2]. One of the most wanted improvements required by the U.S. National Transportation Safety Board is to minimize the dangers of aircraft flying in icing conditions. The current research on freezing rain and large water droplets could revise the way that aircraft is designed and approved for flight in icing conditions, as well as provide to the flight crews accurate information to quickly recognize dangers of all types of icing, such that they maintain airspeeds, which can avoid loss of aircraft control [3]. The different concepts for aircraft wing de-icing developed so far may be classified as thermal, fluid, and mechanical. The thermal systems use thermal energy to heat the ice-covered surface. The fluid systems are based on fluid injection through tiny holes on the surface, which either melts the ice or prevents the accretion. The mechanical systems use mechanical energy to cause deformation of the affected surface, which results in ice cracking and debonding; they can be pneumatic, piezoelectric, vibratory, and electroimpulse de-icing (EIDI) systems.

The principle of the EIDI system is quite simple: a system of inductive coils, which act as mechanical actuators, is placed in an array near the inner leading edge surface. The coils are fastened either directly on the airfoil section or on the spars, as shown in Fig. 1. The discharging of electric capacitors triggers the coils generating an electromagnetic field, which induces electric current in the metallic airfoil surface. The final result of the magnetic field is a mechanical impulsive loading, which sets the leading edge (LE) skin to mechanical vibration that causes fracture and debonding of the accreted ice.

The EIDI system potentially meets the basic ice protection requirements, such as low power requirements (EIDI requires less than 1% of the power required for hot air or electrothermal anti-icing system), weight comparable to other de-icing systems (from around 30 kg for a small six-place aircraft to about 250 kg in a 250-passenger aircraft) [4], high efficiency for aircraft and helicopters with relatively small power margins and is preferable from the usual hot-air systems in the case of high-speed turboprop or high-bypass engines [5]. One disadvantage of the EIDI system is that its effectiveness is dependent on the geometry of the airfoil section. As reported in [6], the LE structures with a radius of curvature smaller than 10 mm are difficult to be de-iced. In addition, the complete de-icing of very high-radius LE structures may be impossible using only one coil per bay. Moreover, structural fatigue problems may appear due to the repetitive impact loading applied during the operation of the EIDI system.

Received 22 November 2005; revision received 17 March 2006; accepted for publication 17 March 2006.

*Assistant Professor, Laboratory of Technology and Strength of Materials, Department of Mechanical Engineering and Aeronautics; labeas@mech.upatras.gr.

†Ph.D. Student, Laboratory of Technology and Strength of Materials, Department of Mechanical Engineering and Aeronautics.

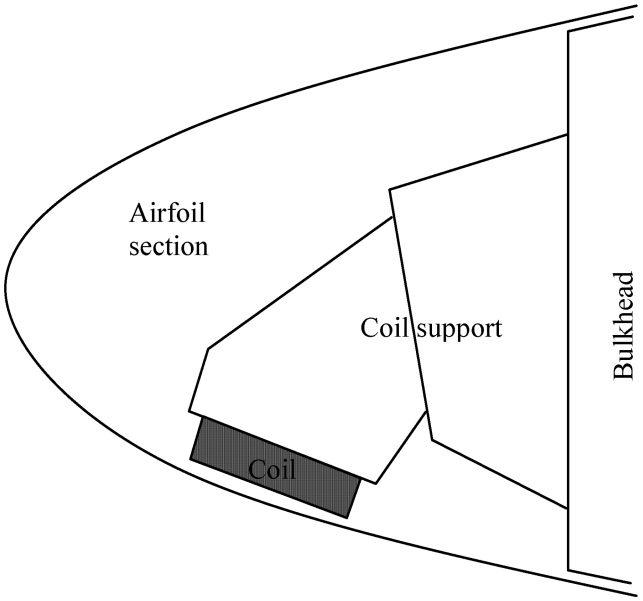

Fig. 1 Coil position and fastening in an EIDI-equipped airfoil section.

According to the literature, the first patents of an EIDI system date back to 1939 [7]. The interest for EIDI systems in Russia resulted in the construction of an aircraft equipped with an EIDI system in the year 1972 [8]. During the same decade the EIDI system was also under investigation in France, England, and the United States, however, it has never been fully developed and widely applied. Most probably this is due to the fact that all the attempts to design such a system were not established on the adequate research of the basic phenomena involved [6], as well as due to the high number of sensitive process parameters, which require very accurate determination and implementation.

Although numerous research projects have been focused on the problem of the aircraft in-flight de-icing (e.g., the NASA LEWICE [9] and the Defence Research Agency TRAJICE [10] programs), most of them deal with the ice accretion phenomenon and the ice physics. Publications specific to the EIDI system, such as [1,4,6,11,12] are restricted to the description of system variations. Only in a few works (i.e., in [5,13–15]), have attempts been made for the numerical simulation of the phenomenon, as well as the establishment of analytical models for the debonding of the ice-metal interface. The first theoretical model of the LE de-icing problem, presented by Khatkhate et al. [5] and Scavuzzo et al. [15], is based on approximate modeling of the ice and the LE structure with shell elements connected by short beam elements of zero mass and large stiffness. This modeling approach results in the calculation of the interface tensile and shear stresses with insufficient accuracy. Furthermore, the ultimate out-of-plane shear stress criterion used in [5,15] to predict the mechanical debonding of ice-metal interface is insufficient to predict de-icing under general circumstances, for example, when subsequent de-icing pulses are applied. In this case, the ice-skin interface is already partially cracked by the initial pulse and the ice is removed due to inertia normal tensile stresses. Lentzos [13] and Kermanidis et al. [14] use the linear elastic fracture mechanics theory and the Griffith criterion to study the ice debonding of a one-dimensional ice-metal cracked interface. Application of this theory to realistic conditions and full-scale LE numerical models requires the assumption of numerous cracked interfaces in the structure, which means huge programming effort and computational cost. Furthermore, the skin fatigue issue, which is one of the most important EIDI drawbacks, has not been investigated so far.

In the present work, a detailed numerical simulation methodology of the de-icing process using the finite element method is presented. A more accurate stress analysis of the ice-skin interface is performed by developing a three-dimensional ice/LE skin model, which enables a more precise determination of the normal and shear interface stresses. The connection of the LE skin surface to the accreted ice is realized by coupling, with adhesive bonds, the LE skin external nodes to the matching nodes of the adjacent ice surface. A de-icing criterion, which takes into consideration both the tensile and shear strengths of the ice-skin interface, is proposed. Each pair of coupled nodes is individually examined for fulfillment of the debonding criterion during the nonlinear transient numerical analysis of the structural model. Local de-icing is realized as breakage of these adhesive bonds and uncoupling of the connected nodes. The calculated skin in-plane stress history induced by the de-icing pulse is used for fatigue calculations.

The developed simulation methodology is initially validated for the case of de-icing an ice-covered flat surface. Modeling issues of the simulation approach are investigated, including the skin and ice discretization density required for accurate interface stresses calculation, the determination of the de-icing equation exponents, and the model capability to successfully predict the de-iced regions. Using the optimum modeling parameters derived for the flat plate de-icing problem, an aircraft wing leading edge section is modeled and its de-icing process is simulated. Using the developed model, the effect of the various parameters on the de-icing efficiency and the skin fatigue behavior has been studied. The investigated parameters include EIDI system characteristics (coil position, coil density, and electrical power), wing LE geometrical features (skin radius and thickness), and ice accretion (ice thickness and coverage). It has been proven that the developed model successfully simulates the electroimpulsive de-icing phenomenon and can be used for the determination of the effect of a high number of interrelated parameters on the system efficiency and structural response.

II. EIDI Simulation Methodology

The most important issues of the electroimpulsive de-icing process simulation of a fully or partially ice-covered surface are: a) the development of an effective finite element (FE) model, which will lead to the precise calculation of the interface and the in-plane stresses, b) the transformation of the electroimpulsive loading to mechanical, and c) the derivation of a reliable ice debonding criterion.

A. Finite Element Modeling

The investigated leading edge model presented in Fig. 2 is based on a typical airliner structural configuration. It includes 13 bays (rib pitches) of a total length of 1.126 m, however, most of the current parametric nonlinear dynamic analyses have been performed using a three-bay LE section, as it was proven that a coil cannot induce considerable deformations beyond its adjacent bay sections. The thickness of the leading edge skin is considered 2 mm, although the detailed description indicates variable skin thickness due to reinforcements at the areas of skin connection to ribs and fuselage. The ice partly or entirely covering the LE skin surface has been considered by laying extra material volumes over the leading edge skin. The ice thickness has been ranged from 4 to 12 mm.

Both the skin and ice structures are modeled as volumes, using the three-dimensional SOLID95 element of the ANSYS FE code [16]. This element type is a structural 20-node higher-order element, which can tolerate irregular shapes without significant loss of accuracy. The shape functions assigned to this element are second-order polynomials, approximating the element edge with a parabolic curve rather than a straight line. Consequently, this element type is capable of calculating the out-of-plane shear stresses τ_{xz} and τ_{yz} with sufficient accuracy. The cost for this higher accuracy is the increase in calculation time. The leading edge ribs and the web of the leading edge spar are modeled with the shell element SHELL63, whereas the spar flanges are modeled by two-dimensional beam elements. The boundary conditions applied to the model aim to represent, as accurately as possible, the real boundary conditions of the section. Considering that the investigated section is located away from the root or the tip of the LE, all nodes of the external ribs are fixed in the longitudinal direction ($UY = 0$) and the corresponding rotations are constrained ($ROTX = ROTZ = 0$). Furthermore, the upper and

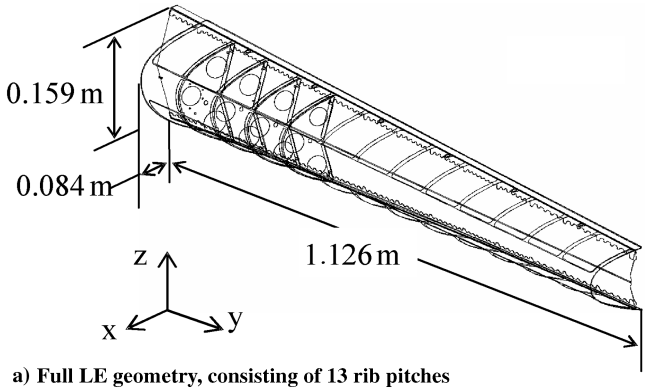

a) Full LE geometry, consisting of 13 rib pitches

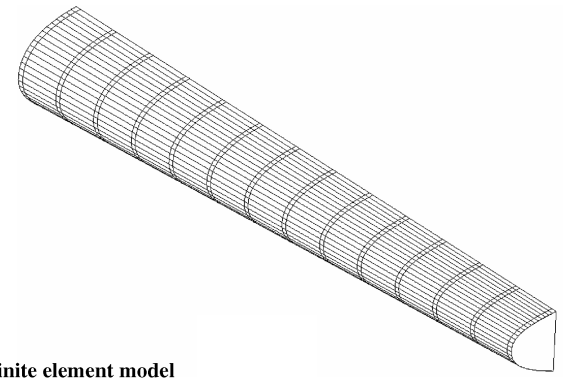

b) LE finite element model

Fig. 2 Modeling the LE geometry.

lower flanges of the LE spar are fixed in the x and z directions, allowing rotation around the spar axes, to better approximate the real support of the skin.

The aluminum skin and the ice material are considered to behave linearly elastic. For the LE skin, Al 2024 material properties are introduced (i.e., $E = 71.5$ GPa, $\nu = 0.33$ and $\rho = 2780$ kg/m^3), whereas for the ice material, the corresponding properties are $E = 5.5$ GPa, $\nu = 0.3$ and $\rho = 897$ kg/m^3.

The de-icing process is divided in short time steps and a nonlinear transient dynamic analysis is performed to compute the displacement, velocity, and acceleration histories, taking into account inertia and damping effects. The debonding criterion is applied at the end of each step to predict the removed ice particles and the FE model is updated accordingly, by deleting the respective elements.

B. Transformation of the Coil Electromagnetic Field to Mechanical Loading

As explained previously, the mechanical impulsive load is invoked by the complex electromagnetic phenomenon. The inductive coil of the EIDI system introduces electric current to the target skin material, resulting in a mechanical load, which has a spatial and transient distribution. The determination of the exact mechanical load produced by the coil, without performing experimental measurements, is a very difficult procedure that requires knowledge of the detailed characteristics of the specific coil, its electrical circuit, the peak electric current in the circuit, and the time-dependent discharging voltage. The studies in [1,6,15,17] explain the principles of transforming the EIDI pulse to mechanical loading.

The most integral study on this phenomenon, presented in [1], establishes a theoretical model for the calculation of the coil-induced peak mechanical force. Measuring the magnetic flux, the authors calculated the current induced in the target material, from which the peak mechanical force $F_{\max}$ (perpendicular to the affected surface) is formulated as:

$$F_{\max} = (I_{\text{coil}})^2 \cdot f(U, t, r, \mu_0) \tag{1}$$

In the present study, the used coil has electric current of 940 A. Using Eq. (1), the peak force induced by the electromagnetic circuit is calculated to be $F_{\max} = 130$ N, with the adoption of the parametric function $f(U, t, r, \mu_0)$, as given in [1]. Having determined the peak force of the mechanical load, its spatial distribution is assumed to be constant at the coil area projected onto the LE skin and decreases linearly to a zero value at a distance 150% of the coil radius. Furthermore, the mechanical force has a duration of 1 ms and its transient distribution follows a sinusoidal function of period T equal to 2 ms, as

$$F = F_{\max} \sin[2\pi t/T] \tag{2}$$

The calculated spatial and transient distribution of the mechanical force is validated hereafter during the modeling evaluation process.

C. De-Icing Criterion

The adhesive metal to ice bond is modeled via coupling of all degrees of freedom at each pair of the adjacent interface nodes. The tied interface nodes are released when the bond strength is exceeded. A failure criterion, similar to those used to check the failure of riveted joints, is developed. The criterion is based on both normal and shear interface stresses, having the form of the following equation:

$$\left(\frac{\sigma_{\max}}{\sigma_U}\right)^a + \left(\frac{\tau_{\max}}{\tau}\right)^b \geq 1 \tag{3}$$

where a and b determine the relative influence of normal and shear stress on the interface failure.

The ultimate normal and shear stresses of the ice-metal interface are difficult to be measured, as they depend strongly on many parameters; therefore, their complete determination for different environmental ice accretion conditions, ranging from LE skin surface roughness to varying ice impact velocities requires huge experimental effort.

In [18] an overview of the efforts on the experimental determination of ice adhesive shear strength is presented, focusing on the specific problem of LE surface de-icing. The influence of all the important parameters on the adhesive shear interface strength is examined. It is concluded that for accretion temperatures from -10 to -5°C and ice layer thickness of around 30 mm, the shear strength increases by increasing wind velocity and surface roughness. The average value of the ultimate shear strength τ_U for all investigated conditions in [18] is around 0.4 MPa, which is the value used in the present work in the debonding Eq. (3).

For the determination of interface normal tensile strength, a wide experimental campaign including three-point bending tests, tensile adhesion tests of an ice layer between two flat aluminum plates, and EIDI tests have been performed in the frame of the Brite–Euram program entitled "Civil Aircraft Protection Against Ice [19]." An important outcome of this investigation, also presented in [20], is the development of a methodology for the production of a repeatable form of ice (control of the ice grain size and porosity), which enables the reliable determination of the ice mechanical properties. The tensile adhesion tests have been performed for accretion temperatures of -2, -8, and -20°C. The tensile strength of the ice adhesive bond was found to range between 0.78 and 1.44 MPa. To make conservative ice removal predictions, the ultimate tensile strength value of 1.44 MPa is adopted for use in the debonding criterion of the current study.

The default values of the coupling parameters a and b of Eq. (3) are unity, implying equal contribution of the normal and shear loading to the interface fracture. In the specific de-icing problem, the importance of the two types of loading changes during the de-icing phenomenon. For the initial interface cracks development, the shear loading is more important, whereas during the phase of ice removal, the normal inertia stress predominates. A parametric study for the determination of the parameters a and b has been performed during

the methodology validation phase and its results are presented in the following section.

III. Simulation Methodology Validation in the Case of De-Icing a Flat Surface

The simulation methodology is initially validated in the problem of de-icing a flat aluminum plate, as it is a smaller size problem compared with the LE structure, therefore, more suitable for validation purposes and for the parametric investigations required for the determination of the simulation parameters. Specifically, the de-icing simulation of a flat plate is used for: a) verification of the process of transformation of the electromagnetic field into mechanical loading; b) determination of the FE mesh density, element types, and especially the required number of elements through the thickness of the ice and LE skin, which is important for the interface stress calculations; c) determination of the debonding criterion coupling parameters; and d) validation of the proposed simulation methodology.

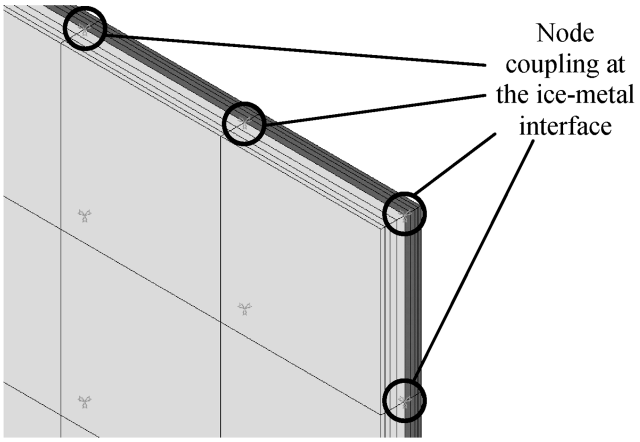

Fig. 3 Degrees of freedom coupling of the adjacent nodes in the ice-metal interface.

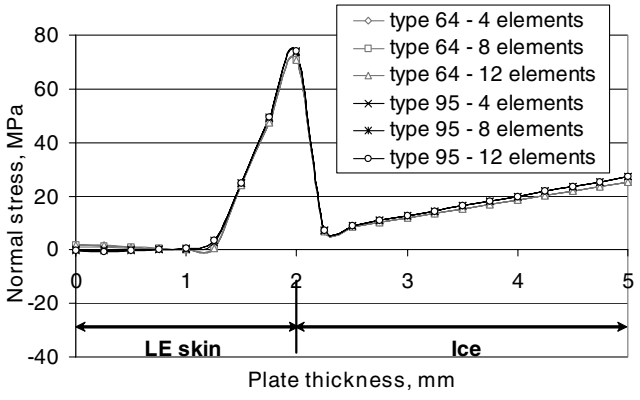

a) Through-thickness normal stress distribution

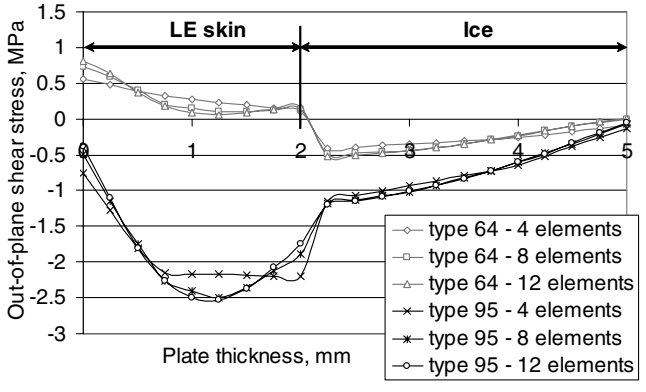

b) Through-thickness shear stress distribution

Fig. 4 Influence of element type and through-thickness mesh density on calculation accuracy.

A square aluminum plate of 420 mm edge and 2 mm thickness, covered with an ice layer of 3 mm thickness is considered. Both the ice and the metallic plate are modeled using high-order SOLID95 elements, having material properties identical to those used in the full LE model. Figure 3 presents a detail of the FE mesh, focused at the coupling interface of the FE model. Two sets of boundary conditions are applied to the plate: clamping of all four sides and clamping of two adjacent sides. The plate is loaded by the pressure load profile described by Eqs. (1) and (2).

In the stage of the FE model development, a parametric study is performed on the required number of elements through the thickness of the two materials. The plate is clamped on two adjacent sides. An electromagnetic coil of 60 mm diameter impulses the plate central area. The normal and shear through-the-thickness stresses for increasing mesh density are calculated and presented in Fig. 4, for the central plate node. It arises that the more elements used through the thickness of the skin, the better results are obtained considering the through-thickness shear stresses, whereas there is no major influence on the normal stresses. On the other hand, the decrease of the solid elements' thickness is limited by the element aspect ratio, which may lead to solution convergence problems. The use of the SOLID95 element type drastically increases the calculation time in comparison to a standard eight-node structural 3-D element (such as SOLID64), which, on the other hand, is unable to accurately calculate the out-of-plane shear stress, as illustrated in Fig. 4. Therefore, a compromise of the element size and the number of the elements through the thickness is needed. It can be concluded from Fig. 4 that modeling of each material by two SOLID95 elements through the thickness leads to satisfactory accurate calculation of the out-of-plane shear stresses, while the required solution times are reasonable.

An additional parametric study is performed for the investigation of the influence of the in-plane element size on the accuracy of the calculated results. Element sizes of 1 and 2 cm are investigated. The diagram in Fig. 5 presents the displacement time history of the central node of the plate for two different element sizes. A small difference is observed between the two displacement time histories.

Consequently, the fully clamped aluminum plate is subjected to one cycle of electroimpulsive loading. The calculated lateral oscillation history at the middle of the plate is presented in Fig. 5 and compared with the experimentally measured values from [21],

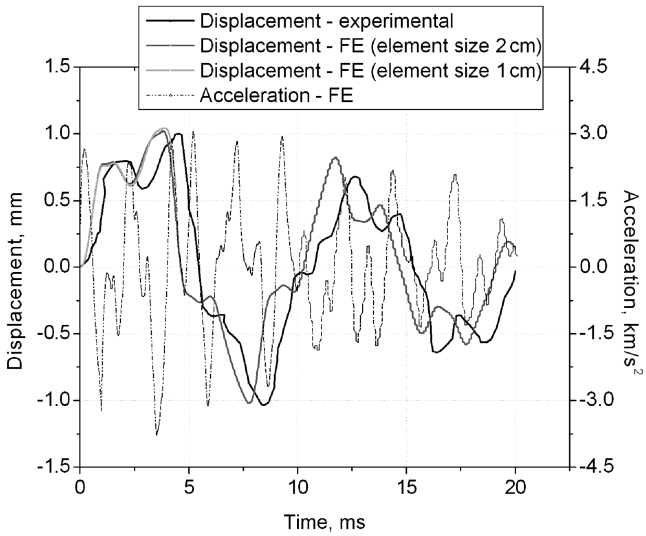

Fig. 5 Acceleration and displacement at the plate center, calculated by 1 and 2 cm elements.

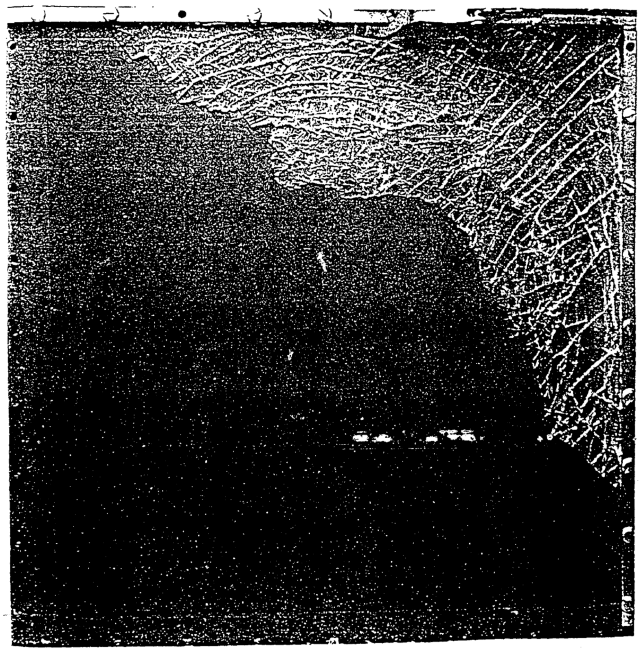

a) Experimental results

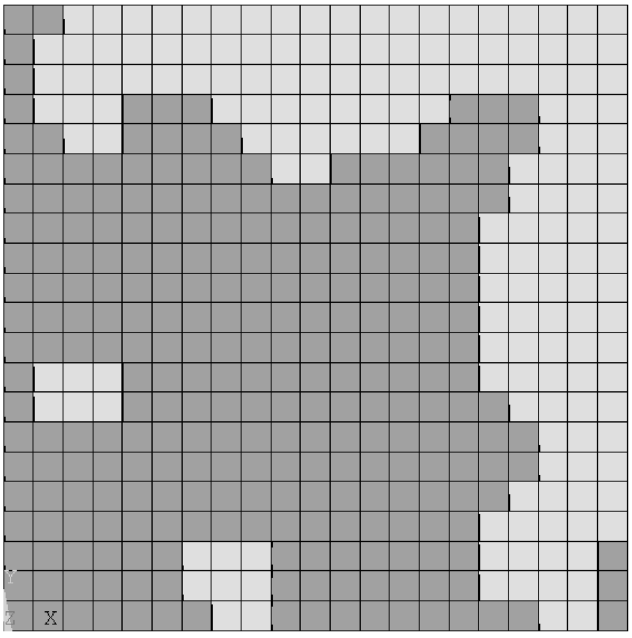

b) Calculated results

Fig. 6 Comparisons between de-icing patterns of a flat plate.

indicating a satisfactory agreement. The calculated central acceleration is depicted, as well, in the same figure.

Having set the mesh parameters, the simulation methodology is evaluated based on the de-icing experiment performed in [21]. The

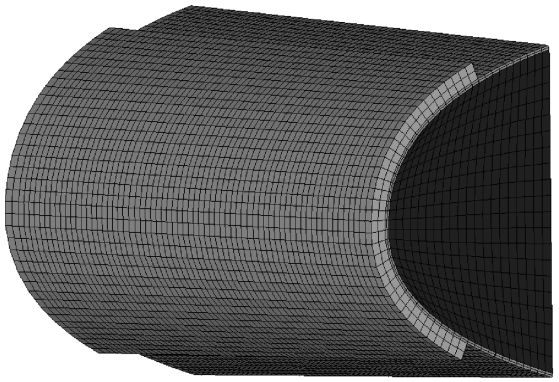

a) Front view

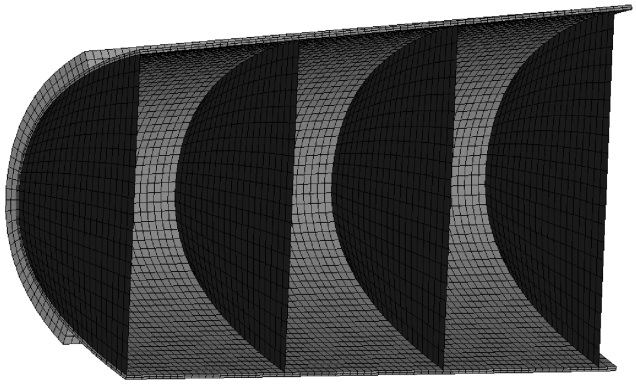

b) Back view

Fig. 7 FE model of the three-bay LE segment with 60% ice thickness.

top and right sides of the plate are clamped on a rigid frame, while the other two sides are left free. The coil is placed at the plate center. In the finite element model, four elements are used through the thickness of the ice and plate structures. Applying the described FE modeling methodology, the experimental test is simulated using a nonlinear transient analysis. After numerous parametric runs, the values of the coupling parameters for the debonding criterion are optimized as $a = 1$ and $b = 2$.

The most important result of the numerical simulation is the predicted pattern of remaining ice on the flat plate, as presented in Fig. 6. Comparing the experimental and the numerically simulated patterns, it may be noticed that the developed modeling methodology reflects the experimental results quite satisfactorily, thus it may be used for prediction of de-icing of more complex geometries such as the aircraft wing leading edge airfoil.

IV. Simulation of the Leading Edge De-Icing Process

The numerical simulation of the de-icing process is performed on the LE segment of three bays, to reduce the calculation time needed for simulating the process on the full LE model. As it is proven after trial numerical simulations using LE segments of 3, 5, and 6 bays and activating only one coil in the middle of the segment, the mechanical load induced by the coil has local character and affects only the adjacent bays, thus the three-bay segment is sufficient for the analysis

Table 1 De-icing parameters investigated and their variations

Parameter	Basic set of parameters		
Ice thickness	60%	80%	100%
Coil position	60%	30%	0%
Ice thickness	8 mm	4 mm	12 mm
Number of coils	Coils in all bays	Coils in first and third bay	Coil in second bay
Load amplitude	100%	50%	200%
Radius of LE curvature	~60 mm	~6 mm	~100 mm

of the de-icing process. The three-bay segment FE model has 8160 solid elements for the LE skin and 1600 shell elements for the LE ribs. Depending on the ice thickness applied, the number of solid elements for the ice structure varies from 5160 for coverage of 60% and up to 8160 for coverage of 100%. The three-bay segment is presented in Fig. 7.

The first objective of the de-icing process numerical simulation of the LE structure is the prediction of the de-icing pattern and specifically the percentage ratio of the de-iced surface over the total LE skin surface. The second and more important objective from the point of view of reduction in weight and power requirements of an EIDI system is the determination of the influence of different system parameters on the de-icing efficiency.

The parameters in question are the ice thickness, the ice thickness, the coil position, number of coils, amplitude of the mechanical force, and the LE radius of curvature.

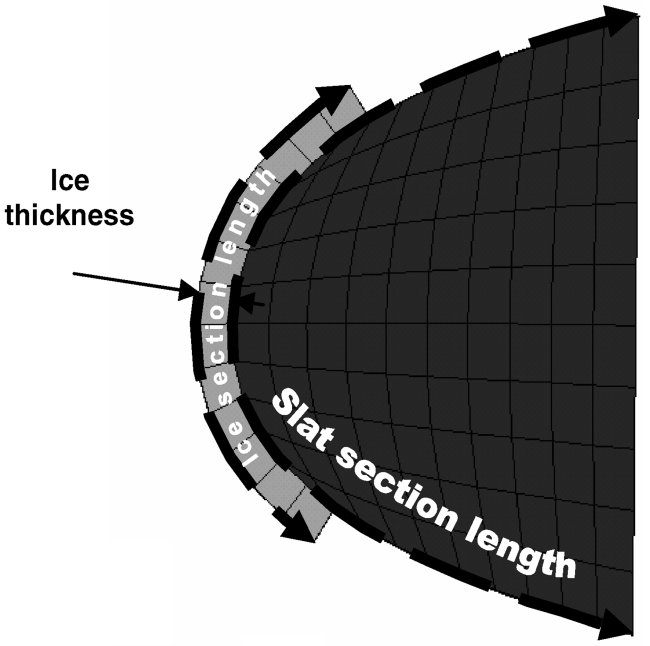

a) Introduction of the ice thickness parameter in the numerical model

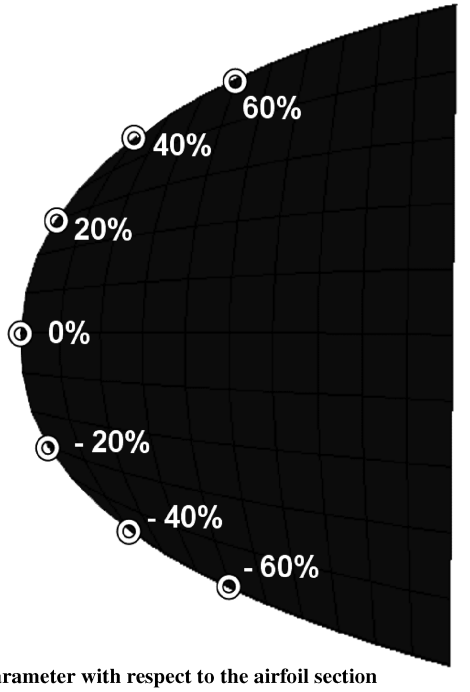

b) Coil position parameter with respect to the airfoil section

Fig. 8 Geometric parameters considered in de-icing FE simulation.

A. Parametric Studies Results

All examined parameters of the de-icing numerical simulation and their variations are presented in Table 1. The set of parameters that corresponds to the basic case is presented in the first column of the table. Only one parameter is varied every time, while the rest keep the basic set values.

1. Ice Thickness

The ice thickness is the ratio of the ice-covered area of the skin over the complete skin area, or, if represented in two dimensions, the ratio of the ice section length over the slat section length [Fig. 8a]. The coverage of ice is applied from the slat apex symmetrically upwards and downwards. The cases simulated comprise the ice thickness of 60, 80, and 100%. The de-icing patterns and percentages obtained from the numerical simulations are presented in Fig. 9. It may be observed that for increasing ice thickness on the LE surface, the EIDI efficiency drop-off is significant. This decrease may be explained if the coil-affected area of a single coil is compared with the ice-covered surface. The coil-affected area remains constant, whereas the ice thickness is increasing, thus the overall de-icing percentage is expected to decrease. The determination of the critical ice thickness, which can be defined as the coverage value for which the complete de-icing of the LE surface is not achieved, is useful for the design of an effective EIDI system.

2. Ice Thickness

To determine the influence of ice thickness on the de-icing percentage, a LE covered with ice of thickness 4, 8, and 12 mm is

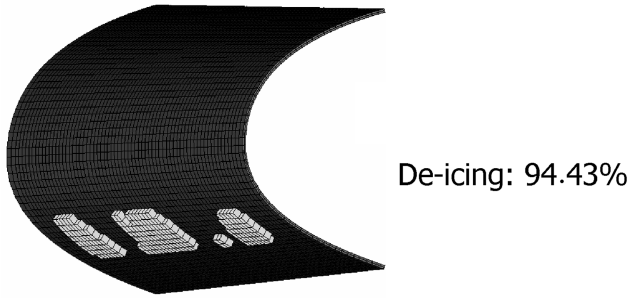

a) Ice thickness: 60%

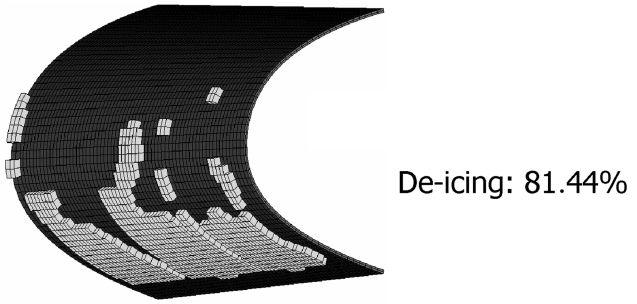

b) Ice thickness: 80%

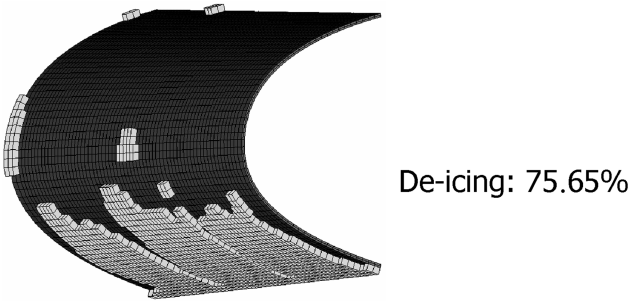

c) Ice thickness: 100%

Fig. 9 Simulated de-icing patterns for different ice thickness percentages.

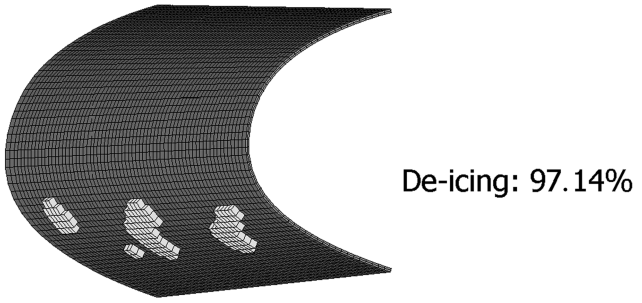

a) Ice thickness: 4 mm

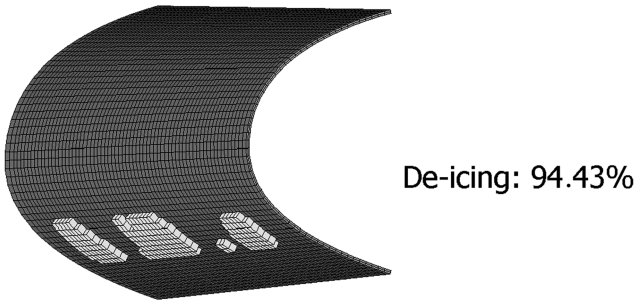

b) Ice thickness: 8 mm

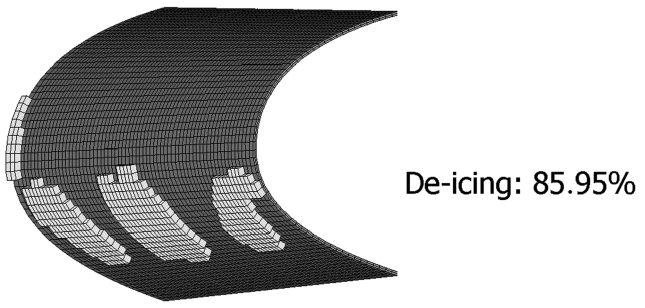

c) Ice thickness: 12 mm

Fig. 10 Simulated de-icing patterns for different ice thicknesses.

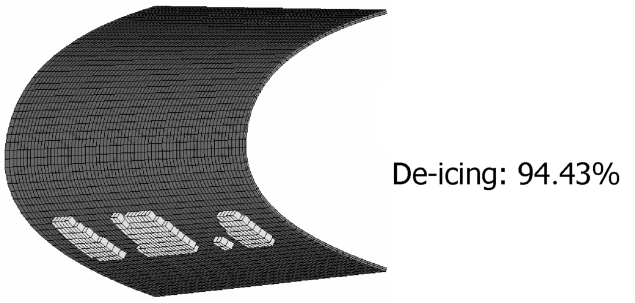

a) Coil position: 60%

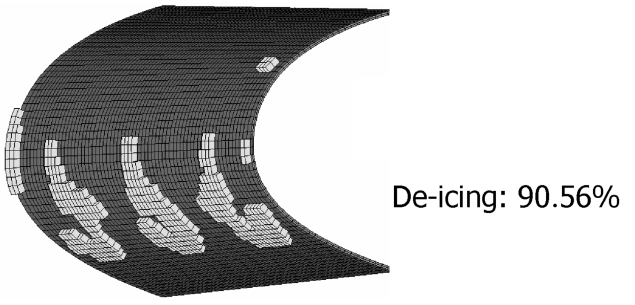

b) Coil position: 30%

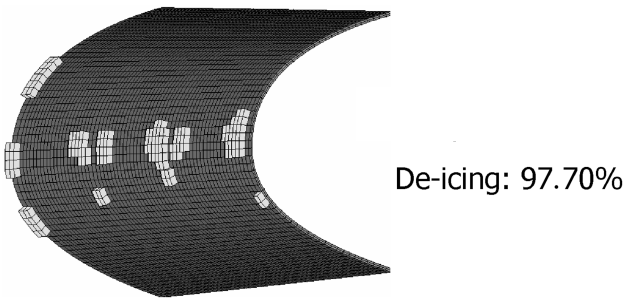

c) Coil position: 0%

Fig. 11 Simulated de-icing patterns for coil positions 60, 30, and 0%.

examined. The simulated de-icing patterns of these three cases are presented in Fig. 10. An examination of the three patterns leads to the conclusion that the de-icing efficiency is higher in the case of thin accreted ice. This qualitative observation is also supported by the respective calculated de-icing percentages (see Fig. 10). The difference in the de-icing efficiency between the 4 and 8 mm ice layers is rather small, but the system efficiency is drastically reduced in the case of de-icing a 12 mm ice layer. This influence may be attributed to the fact that an increase of the ice thickness increases the mass of the ice LE system, which reduces the amplitude of vibration caused by the EIDI system. It should be mentioned that the observed trend of increasing de-icing efficiency with increasing ice thickness is not always valid, as some icing tunnel experimental observations have shown that in certain cases, de-icing becomes more difficult for thin ice layers. Such a case can occur when a thin water layer is trapped between the ice and the surface of airfoil, resulting in a significant damping of the mechanical pulse. This case has not been studied by the present model due to lack of available strength data for the certain case of impact ice formation.

3. *Coil Position*

A very important system parameter is the position of the coil with respect to the airfoil profile. Specifically, the LE radius of curvature at the profile location that the coil is placed plays a major role in the propagation of the oscillatory waves induced by the EIDI impulse, which strongly affect the vibratory mode shapes of the LE structure and thus the system efficiency. The coils are assigned a percentage value indicating the position of the coil relative to the LE apex [Fig. 8b]. For example, the position 0% means that the coil is positioned at the LE apex, the position 50% indicates the point at the airfoil section halfway between the LE apex and LE root, and the position 100% is assumed at the LE root. The positions that are examined are 60, 30, and 0%. The position of the coil with respect to the longitudinal direction of the bay ribs (x axis in Fig. 2) is not varied in the current study, considering the coil placed at the midribs distance. The de-icing patterns obtained from the simulation of these three cases are shown in Fig. 11. It can be noticed that the highest value of de-icing is obtained for the coil position at the LE apex (0%). A slightly lower de-icing percentage is predicted at the 60% position, where the curvature radius is significantly higher from the one at the apex. The lowest de-icing percentage value corresponds to the position near the LE apex (30%).

4. *Number of Coils*

Regarding the possibilities for weight reduction of EIDI systems, it is also important to determine the minimum number of coils required in the LE, that is, whether it is necessary to place a coil in every bay of the leading edge; if the coil-affected area crosses the boundaries of a single bay, a coil in every second or third bay could also give satisfactory results and also reduce system weight by two or three times. Initially, the coils are assumed in every bay of the LE structure. The second case studied is the placement of two coils, one in the first and one in the third bay of the three-bay segment, to examine whether the de-icing efficiency is still satisfactory despite

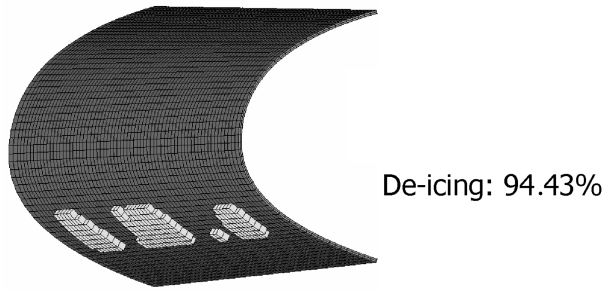

a) Coil in every bay (three coils)

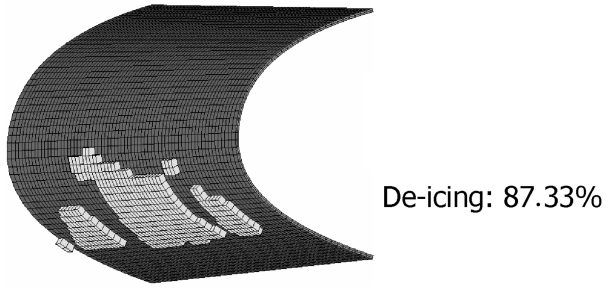

b) Coil in first and third bay (two coils)

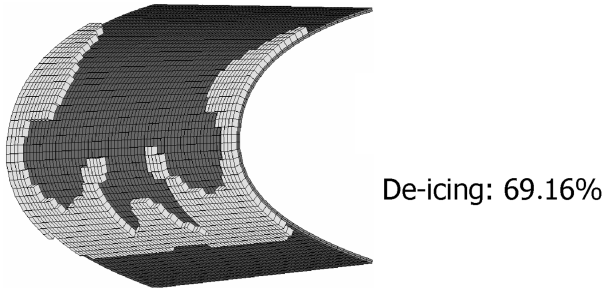

c) Coil in second bay (one coil)

Fig. 12 Simulated de-icing patterns for different numbers of coils applied.

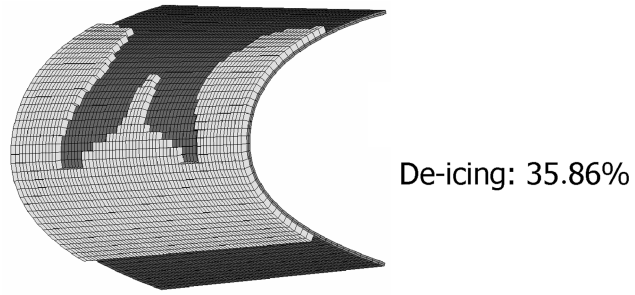

a) Force amplitude: 50%

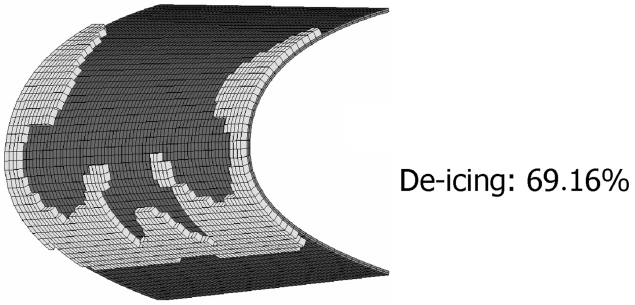

b) Force amplitude: 100%

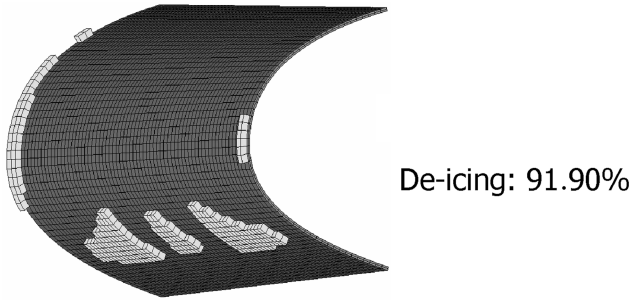

c) Force amplitude: 200%

Fig. 13 Simulated de-icing patterns for different amplitudes of coil-induced mechanical force.

the lack of the middle-bay coil. The third case, that is, the placement of a single coil in the midbay of the three-bay segment, is used to determine the area affected by a single coil. The de-icing patterns simulated for these three cases, as well as the de-icing percentages, are presented in Fig. 12. As expected, the de-icing percentages show that the most efficient system is the one with a coil in every bay. However, the system efficiency has a serious drop-off of around 25% in comparison to the initial configuration if only a single coil is placed in the middle bay. The de-icing pattern of the third case shows that a single coil affects the larger part of the bay where it is placed, but also a significant area of the neighboring bays. The placement of two coils, one in the first and one in the third bay, slightly reduces the efficiency. This configuration leads to an efficiency drop of about 7% in comparison to the initial configuration, which may be considered small, and this deficiency could be eliminated by adjusting some of the other influential parameters toward a lighter system design.

5. *Force Amplitude*

The influence of mechanical load amplitude is investigated because higher loads are expected to expand the coil-affected area and improve the efficiency of the EIDI system. The evaluated force amplitude value, which has been used in the previous simulations, is scaled in a first case to half, whereas in a second case it is doubled. The simulations are performed by activating only one coil in the middle bay of the LE segment, in order to emphasize the effect of this parameter. The effect of different values of force amplitude on the efficiency of the EIDI system is observed qualitatively in Fig. 13, in which the de-icing patterns on the LE are presented. As expected, these figures depict that the efficiency of the EIDI system becomes higher as the mechanical force amplitude grows. This dependence is almost linear, as can be noticed from the de-icing percentages. The results also show that the reduction in the number of coils required for efficient de-icing may be possible, but on the other hand, this means that the energy requirements will be higher in order to produce higher force amplitudes. A detailed study on these two requirements would result in the optimal configuration of the EIDI system.

6. *Radius of Curvature*

The radius of the LE curvature is also an influential parameter, as reported in [6]. To study the effect of the LE geometry on the de-icing efficiency of the applied EIDI system, the initially adopted LE geometry is modified in a way that the leading edge length and depth are kept constant, while the leading edge height is varied, thus producing variations in the curvature of the leading edge. Besides the initial LE geometry, which has a radius of curvature of around 60 mm, two geometries with curvature radii of 6 and 100 mm are studied. The predicted de-icing patterns for these three structures are shown in Fig. 14.

It can be observed from Fig. 14 that LE structures with a radius less than 10 mm may be difficult to de-ice. This may be understood, as for LEs with a sharp radius of curvature, the structure generally becomes much stiffer than a bulbous one, which results in higher resistance in displacement and less ability for transferring the oscillatory waves from one side of the LE surface to the other, making de-icing almost impossible. This is also confirmed by the experimental observations of [6] that a reduction of the curvature radius to less than 10 mm can cause a significant efficiency drop-off of the EIDI system. As the radius of curvature increases, the de-icing efficiency also increases

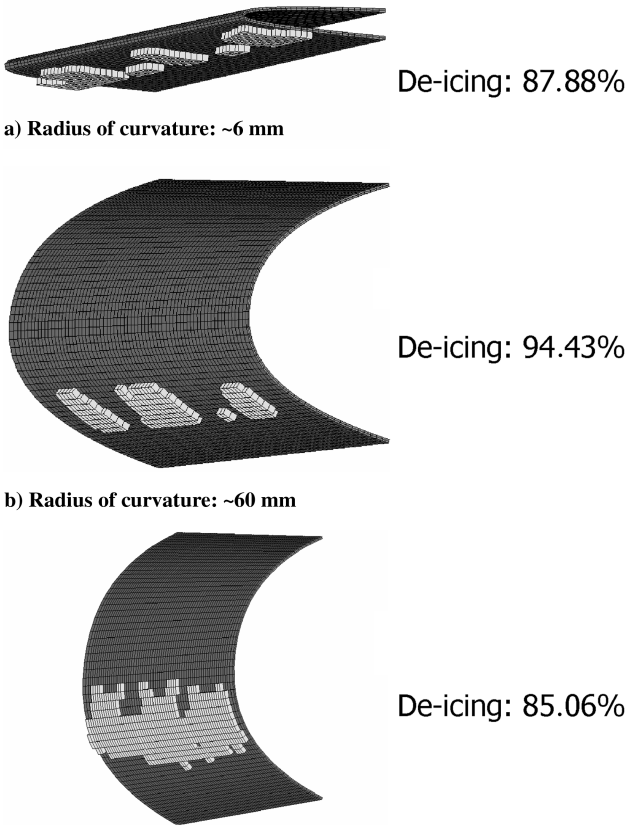

a) Radius of curvature: ~6 mm

b) Radius of curvature: ~60 mm

c) Radius of curvature: ~100 mm

Fig. 14 Simulated de-icing patterns for different LE curvature radius values.

(see Fig. 14, middle pattern). However, when the radius of LE curvature reaches very high values (e.g., 100 mm), a decrease in the de-icing efficiency compared with the initial geometry is exhibited; as the area covered with ice becomes large, the inertia of the ice-skin system increases, and a complete de-icing may be impossible by applying only one coil per bay. In this case, the application of an extra coil in the bay should be considered.

B. Fatigue Investigation

One of the possible disadvantages of EIDI systems in comparison to thermoelectrical or hot air systems is the fatigue problems that can arise for the skin material due to the repetitive impulsive mechanical load. This is a problem that may occur in the regions where the frequent use of the EIDI system is needed. For the basic simulation case (see Table 1) it is calculated that the maximum in-plane normal stresses in the LE skin occur at the coil location and have values of about 160 MPa. The calculated maximum stress history is presented in Fig. 15, from which it can be noticed that after the primary stress peak, which coincides with the coil discharging, a secondary peak is noticed with stress amplitude of around 50 MPa. It is estimated in [1] that the use of the EIDI system in normal flights results in about 15,000 impulses in 20 years. Having in mind the fatigue properties of the aluminum alloy Al 2024 and applying the Miner law for damage accumulation with these magnitudes of the normal in-plane stress, it can be calculated that the damage accumulated after projected 15,000 loading cycles is less than 1% of the damage to failure, therefore, the estimated number of cycles is too low to invoke the LE skin failure due to fatigue. This is proven also by the fatigue tests in [1]. However, in the mentioned fatigue tests, after about 11,500 cycles, a failure occurred in a sheet metal bracket that was connecting the coil beam to the rib. This indicates that, for the fatigue analysis of the EIDI equipped wing LE structure, a detailed modeling approach is needed that will take into consideration the dynamics of the coil itself as well as its connection to the LE structure.

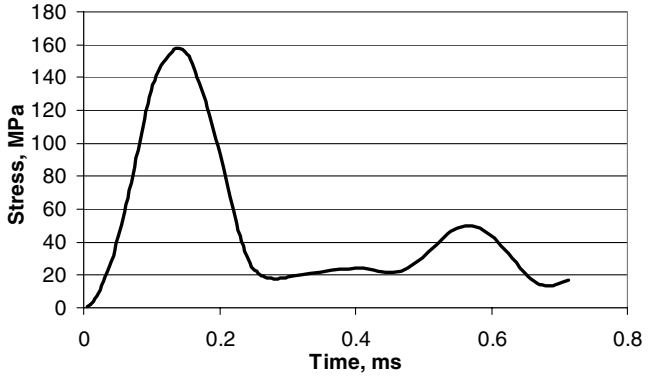

Fig. 15 The LE skin in-plane normal stress time history.

It has to be noticed that the preceding fatigue analysis is based on the in-plane stresses introduced to the skin due to the EIDI pulse of the basic case (see Table 1). However, the system efficiency as shown is not satisfactory for every possible de-icing situation. It is apparent that the strong mechanical pulse required for difficult de-icing cases to remove the accreted ice may raise the stresses developed in the structure beyond its endurance strength, thus fatigue or even immediate failure may occur.

V. Conclusions

A numerical methodology for simulation of the de-icing process of LE structures by the electroimpulse de-icing (EIDI) system is presented in the current work. The methodology is based on an improved interface stress analysis and a global criterion for de-icing due to ice-metal interface failure, employing both the out-of-plane shear and normal stresses. The validity of the proposed criterion is demonstrated in the example of de-icing a flat square aluminum plate. The de-icing experimental test is simulated numerically using an implicit FE code. The comparison shows that the experimentally obtained and the numerically calculated de-icing patterns are in very good agreement, thus proving that the new de-icing criterion is valid for application in the numerical analysis of the de-icing process.

Further on, the developed methodology is applied to a real wing LE geometry for the prediction of de-icing using an EIDI system. A parametric study is performed to assess the influence of the important LE, ice, and system parameters on the efficiency of the EIDI system. The parameters covered by the present study are the ice thickness, ice thickness, coil position, number of applied coils, amplitude of the coil-induced mechanical force, and radius of the LE curvature. Results of the parametric study are obtained in the form of de-icing patterns and percentages of the de-iced surface. It is concluded that the growth of the ice parameters (ice thickness and coverage) causes the reduction in the EIDI system efficiency. In general it is concluded from the parametric studies that each EIDI system design parameter has important influence on the system efficiency and should be taken into consideration. The position of the coil with respect to the airfoil profile is shown to have major influence on the de-icing percentage, with the highest efficiency occurring when the coil is placed at the LE apex position. The LE shape, that is, the radius of curvature, also influences the de-icing efficiency, indicating that for a small radius (under 10 mm), total de-icing may be impossible, whereas for an extremely large radius, the application of more than one coil per bay is required. The LE skin surface area affected by a single coil is shown to be closely related to the amplitude of the EIDI pulse. For the three-bay segment of the LE, the application of only one coil in the midbay is insufficient, but this may be reversed if a higher force value is induced by the coil, as shown from the study on the force amplitude. This also implies that the weight requirements reduction, invoked by less coils applied, causes the rise in the energy required for the effective de-icing. The optimal configuration of the EIDI

system is roughly a result of a compromise between de-icing efficiency, mass, and energy requirements, and depends on the specific needs. The fatigue investigation showed that no fatigue failure is expected in the LE skin in the case of normal de-icing conditions.

Acknowledgments

The authors wish to acknowledge the European Union for their financial support to this research. The results presented in this paper are partially obtained in the frame of the European Union funded research program "Power Optimized Aircraft–POA."

References

[1] Zumwalt, G. W., Schrag, R. L., Bernhart, W. D., and Friedberg, R. A., "Electroimpulse De-Icing Testing Analysis and Design," NASA CR-4175, Sep. 1988.

[2] Lynch, F. T., and Khodadoust, A., "Effects of Ice Accretions on Aircraft Aerodynamics," *Progress in Aerospace Sciences*, Vol. 37, No. 8, 2001, pp. 669–767.

[3] Anon., "Reduce Dangers to Aircraft Flying in Icing Conditions," *Most Wanted Transportation Safety Improvements–Federal Issues: Aviation* [online bulletin], National Transportation Safety Board Recommendations and Accomplishments, http://www.ntsb.gov/Recs/mostwanted/air_ice.htm [cited on 17 November 2005]. (This bulletin is online only.)

[4] Heinrich, A., Ross, R., Zumwalt, G., Provose, J., Padmanabhan, V., Thomson, J., and Riley, J, "Aircraft Icing Handbook," Federal Aviation Administration, Rept. ADA238 040, Mar. 1991; also U.S. Department of Transportation DOT/FAA/CT-88/8-2, Vols. 1, 2, and 3.

[5] Khatkhate, A. A., Skavuzzo, R. J., and Chu, M. L., "A Finite Element Study of the EIDI System," AIAA Paper 88-0022, Vol. 26, 1988, pp. 1–8.

[6] Zumwalt, G. W., and Friedberg, R. A., "Designing an Electroimpulse De-Icing System," AIAA Paper 86-0545, 1986, pp. 1–8.

[7] Goldschmidt, R., British Patent Specification No. 505,433, filed 5 May 1939.

[8] Levin, I. A., "USSR Electric Impulse De-Icing Design," *Aircraft Engineering*, July 1972, p. 7.

[9] Ruff, G. A., and Berkowitz, B. M., "User's Manual for the NASA Lewis Ice Accretion Prediction Code (LEWICE)," NASA CR-185129, May 1990.

[10] Gent, R. W., "TRAJICE2–A Combined Water Droplet Trajectory and Ice Accretion Prediction Program for Aerofoils," Defence Research Agency, RAE-TR-90054, November 1990.

[11] Masters, C. O., "Electroimpulse De-Icing Systems: Issues and Concerns for Certification," AIAA Paper 89-0761.

[12] Nelepovitz, D. O., and Rosenthal, H. A., "Electroimpulse De-Icing of Aircraft Engine Inlets," AIAA Paper 85-0546.

[13] Lentzos, G., "Mechanical Debonding of Bi-Layer Materials," Ph.D. Dissertation, Laboratory of Technology and Strength of Materials, Dept. of Mechanical and Aeronautical Engineering, Univ. of Patras, Greece, 1995.

[14] Kermanidis, Th., Lentzos, G., Pantelakis, Sp., and Hammond, D., "A Mechanical Model to Investigate Airfoil De-Icing Mechanics," *Zeitschrift für Flugwissenschaften und Weltraumforschung (Journal of Flight Sciences and Space Research)*, Vol. 19, No. 4, 1995, pp. 299–306.

[15] Scavuzzo, R. J., Chu, M. L., Woods, E. J., Khatkhate, A. A., and Raju, R., "Finite Element Studies of the Electro Impulse De-Icing System," *Journal of Aircraft*, Vol. 27, No. 9, 1990, pp. 757–763.

[16] ANSYS, FE Software Package, Release 8.1, ANSYS, Canonsburg, PA, 2004.

[17] Bernhart, W. D., and Schrag, R. L., "Electroimpulse Deicing: Electrodynamic Solution by Discrete Elements," *Journal of Aircraft*, Vol. 26, No. 6, 1989, pp. 547–553.

[18] Chu, M. C., and Scavuzzo, R. J., "Adhesive Shear Strength of Impact Ice," *AIAA Journal*, Vol. 29, No. 11, 1991, pp. 1921–1926.

[19] Anon., "CAPRI—Civil Aircraft Protection Against Ice," Brite–Euram, Project Ref. AERO0008, Mar. 1990–Mar. 1992.

[20] Esposito, S., and Riegel, E., "Ice Adhesion Tests," Alenia Rept. CAPRI/AIT/REP/2415/01/REV, 1992.

[21] Hammond, D. W., Braund, M. J., and Duffy, P., "Progress Report on Ice Physics Investigation," British Aerospace Rept. CAPRI/BAE/REP/0807/SUB, Nov. 1990.